Article

ZnO-ZnS Heterostructure as a Potent Photocatalyst in the Preparation of Some Substituted Chromenes and Remarkable Antigastrointestinal Cancer Activity

Liqing Liu, Longgang Wang, Dong Sun, Xu Sun, Luguang Liu, Weizhu Zhao, Reza Tayebee, and Bing Liu*

Read Online

ACCESS | Metrics & More | Article Recommendations

R_1 = NO$_2$, F, Cl, Br, H, CH$_3$, OCH$_3$,
R_2 = H, CH$_3$
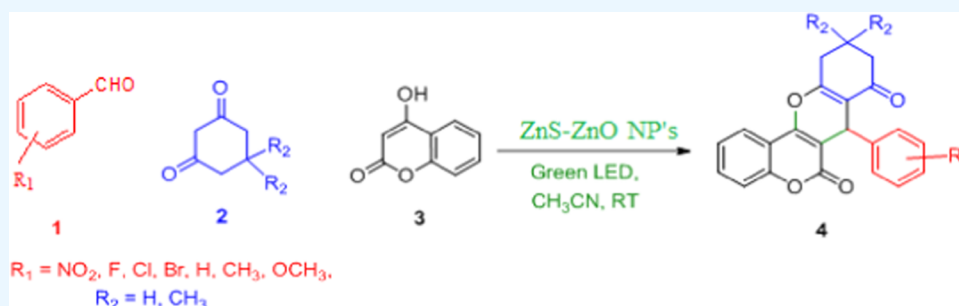
ABSTRACT: The nanosized hybrid material ZnO-ZnS was synthesized using the well-known sol−gel method, as a simple and environmentally friendly procedure. The material was then characterized using various techniques including FESEM, TEM, UV−vis, DRS, EDS, XRD, and FT-IR. The characterization studies revealed the generation of ZnO-ZnS nanoparticles with a mean size of around 25 nm. Moreover, DRS analysis provided a band gap of 3.05 eV for this nanomaterial. The photocatalytic properties of the ZnO-ZnS heterojunction was investigated in the synthesis of some substituted chromenes under mild reaction conditions. The results showed that the prepared nanophotocatalyst exhibits significantly higher activity compared to its individual components (ZnO and ZnS) and provides 73−87% yield with 0.01 g of ZnO-ZnS after 30 min. In addition, the nanophotocatalyst demonstrated a high reusability in the desired condensation reaction. The enhanced photocatalytic activity of ZnO-ZnS can be attributed to the slower recombination of the electron−hole pairs in this semiconductor material. The reactive species OH$^\bullet$, $^\bullet$O$_2^-$, and h$^+$ are believed to play important roles in the photocatalytic system. Furthermore, cellular toxicity of ZnO-ZnS nanoparticles was evaluated on HCT-116 human gastrointestinal cancer cell line by MTT assay. The results proved a distinct reduction of cell viability, proofing cytotoxicity of nanoparticles on the cancer cells. This study highlights the potential of the nanoparticles against gastrointestinal cancer.

1. INTRODUCTION

Fabrication of visible-light-responsive photocatalysts is one of the most promising research topics in the field of photocatalysis due to the green features of this route and the utilization of abundant solar energy. Zinc oxide (ZnO) is a cost-effective semiconductor with low toxicity and a wide band gap of 3.37 eV, making it suitable for various applications in both industry and academia.[1] Zinc sulfide (ZnS), with a wide band gap of 3.72 eV, has emerged as one of the most promising materials for junction formation with ZnO.[2] However, these pristine photocatalysts face the high electron−hole recombination rate and severe photocorrosion. Therefore, fabrication of the semiconducting heterojunctions is a preferred solution to improve the photocatalytic performance of zinc oxide.[3,4] The coupling of semiconductors not only enhances their individual characteristics but also facilitates

efficient separation of the photogenerated hole−electron pairs, extends photoabsorption, and provides strong redox potential.[5] In this view, to enhance the photocatalytic performance of ZnO through utilization of visible-light and reduction of charge−carrier recombination, efforts have been devoted to coupling of ZnO with other semiconductors.[6−9]
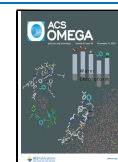
In recent years, researchers have successfully fabricated heterostructure semiconductors such as TiO$_2$/SrO, CdS/TiO$_2$, CdS/ZnO, CdS/AgI, CdS/ZnS, Cd$_3$P$_2$/TiO$_2$, AgI/Ag$_2$S,

Scheme 1. General Scheme for the Synthesis of Substituted Chromeno[4,3-b]chromenes
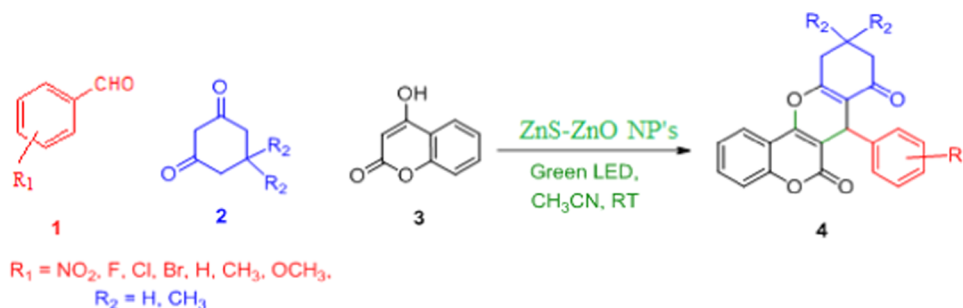
Cd$_3$P$_2$/ZnO, ZnO/ZnSe, SnO$_2$/CdS, SnO$_2$/TiO$_2$, CdSe/TiO$_2$, and Cu$_2$S/CdS.[10−13] These heterostructures exhibit unique structural features, and their properties have been extensively studied. Overall, the exploration of heterojunctions involving zinc oxide and other semiconductors offers exciting opportunities to tailor and enhance the functionalities of ZnO and achieve diverse applications in optoelectronic, catalysis, and energy conversion.[14−17]

Chromenes play a pivotal role as key components in various biologically active materials because of their hybrid heterocyclic structure.[18−20] These compounds offer a diverse range of biological activities, including antimicrobial and anticancer effects. Moreover, the use of chromenes as drugs in the gastrointestinal field is an area of ongoing research because of their anti-inflammatory and antioxidant properties. These characteristics make them potentially useful in the treatment of gastrointestinal disorders and gastric ulcers, where inflammation and oxidative stress are important. Given the nontoxic nature of chromenes and their broad pharmacological importance, chemists have been motivated to explore more efficient synthetic routes for these chemicals.[21] While new methods are developed for the preparation of substituted chromenes, certain deficiencies in terms of environmental impact and economic viability have driven academic researchers to develop advanced and more effective approaches to synthesize these compounds.

Visible light photocatalysis represents a promising avenue for driving diverse organic transformations with the aid of an appropriate photocatalyst.[22] The exploration of various semiconductors has significantly contributed to advancing knowledge in the chemical industries, artificial ion batteries, optoelectronics, and photocatalysts. Notably, ZnO-WO$_3$, CuO/WO$_3$/TiO$_2$, ZnO-TiO$_2$, ZnO/CeO$_2$, ZnO/CuCo$_2$O$_4$, ZnO/BiVO$_4$, and ZnO-In$_2$O$_3$ have emerged as effective photocatalysts for numerous transformations under common light irradiation sources.[15,23−29] We believe that the development of a ZnO-ZnS heterostructure could enhance electronic transitions within a broad energy range, thus establishing it as a novel and efficient photocatalyst. Herein, ZnO-ZnS is prepared via a simple hydrothermal-based chemical sol−gel method that requires no special requirement. The chemical method used in this study to prepare the ZnO-ZnS heterojunction photocatalyst offers several advantages over other methods such as controlled composition and stoichiometry, uniform distribution, and homogeneous dispersion of ZnO and ZnS components in the heterojunction photocatalyst, and versatility in terms of the materials used to prepare the final photocatalyst. Then, the fabricated photocatalyst was utilized in the multicomponent synthesis of some substituted chromeno[4,3-b]chromenes (Scheme 1).

2. MATERIALS AND METHODS

2.1. Materials and Methods. This research used pure materials and solvents obtained from commercial resources and performed without further purification. Morphology studies were conducted using FESEM, Mira 3-XMU, and a TEM (PHILIPS TECNAI 10) equipped with an EDS (energy-dispersive X-ray) analyzer. FT-IR spectra were obtained by using a Fourier transform 8700 spectrophotometer. UV−visible spectra were captured by using a Photonix UV−vis instrument. The UV−vis diffuse reflectance spectra (UV−vis DRS) obtained from a UV−vis Scinco 4100 spectrometer. Spin coating was used to prepare thin films of ZnO-ZnS. Therefore, a solution of ZnO-ZnS was deposited onto a silicon film by using a spinner. Then, the substrate was rotated at a high speed to spread the solution uniformly and form a thin film as the solvent was evaporated. PXRD analysis was performed on an X'Pert MPD instrument equipped with Cu (Kα radiation) at 0.030 A and 40.000 eV, with a scanning rate of 3° min^{-1} within the 2θ range of 5−80°.

2.2. Sol−Gel Preparation of Zinc Oxide Nanoparticles. The experiment began by sonication of a 50 mL ethanol solution (99.7%) of zinc acetate dihydrate (Zn-(CH$_3$COO)$_2$·2H$_2$O, 3.30 g, 15 mmol, 99.8%) with a concentration of 0.3 M for a duration of 35 min using an ultrasonic cleaner. Subsequently, a 50 mL aqueous solution of urea (CO(NH$_2$)$_2$, 0.90 g, 15 mmol, 99.6%) with a concentration of 0.3 M was gradually added dropwise to the zinc acetate solution while vigorously stirring. Following this step, a 0.5 M aqueous solution of sodium hydroxide pellets (99.8%) was slowly incorporated into the above solution with continuous vigorous stirring until a pH of 11 was achieved. Once the desired pH was attained, the reaction mixture was refluxed at a temperature of 85 °C for 1.5 h. After the refluxing period, the resulting precipitate was naturally cooled down and then subjected to filtration. The filtrate was washed multiple times with deionized water to eliminate impurities. Finally, the precipitate was washed with acetone until neutralization and subsequently dried at 80 °C to obtain the final product.

2.3. Synthesis of Zinc Sulfide Nanoparticles. Zinc sulfide (ZnS) was synthesized by using a straightforward method employing zinc acetate and sodium sulfide. In the standard procedure, a 10 mL solution of 1 M sodium sulfide (Na$_2$S, 1.26 g, 10 mmol, 99.7%) was carefully added drop by drop to a 10 mL solution of 1 M zinc acetate dihydrate (Zn(CH$_3$COO)$_2$.2H$_2$O, 2.19 g, 10 mmol, 99.8%), while stirring at 80 °C. Subsequently, the resulting product was isolated through centrifugation and subjected to drying at 80 °C for 1 h and, finally, ground into a fine powder. The
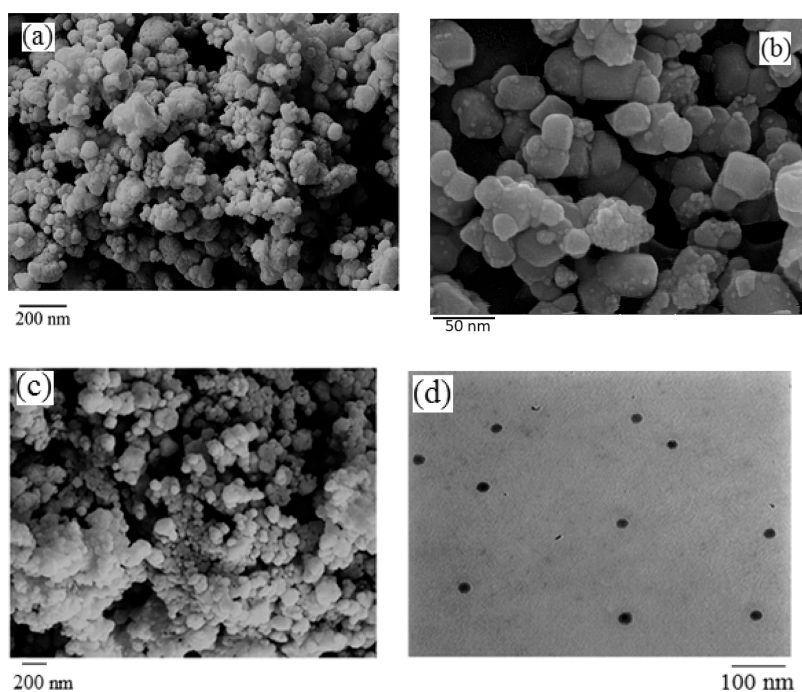
Figure 1. FESEM images of pristine ZnO (a), ZnS (b), and ZnO-ZnS (c) and TEM micrograph of ZnO-ZnS (d).

unwanted sodium and sulfate ions were removed by repeated washing and centrifugation.

2.4. Preparation of the ZnO-ZnS Nanomaterial. To prepare the ZnO-ZnS nanomaterial, the above-prepared nanoparticles were taken at the same molar ratio and ground to obtain a homogeneous mixture. Then, the mixture was placed in a crucible and annealed in a furnace at 550 °C for 3 h. Finally, the annealed material was cooled to room temperature and ground again to get the nanocrystalline ZnS-ZnO structure.

2.5. General Procedure for the Synthesis of Chromenes. In a small test tube, benzaldehyde, dimedone, and 4-hydroxycoumarin (1 mmol each one) were mixed with 0.01 g ZnS-ZnO in 5 mL of acetonitrile. The mixture was magnetically stirred while illuminated by a green laser at room temperature on air. Once the reaction was complete, the mixture quenched with 10 mL of water. Next, the undissolved species were separated by filtration and the separated solids were transferred to a new test tube involving ethyl acetate (EtOAc). The ZnO-ZnS was separated easily to produce a clear solution containing chromene product. To remove any remaining moisture, the organic part involving chromene was dried over anhydrous sodium sulfate. Finally, the crude chromene was purified by column chromatography to attain the pure final product.

2.6. Cancer Cell Culture. The HCT-116 cell line was obtained commercially. The cells were cultured and maintained in a well-known Minimum Essential Medium (MEM), supplemented with 10% fetal bovine serum, 1% glutamine, and a 1% penicillin-streptomycin antibiotic solution. To initiate subculturing, the cells were trypsinated using trypsin-EDTA solution and subsequently seeded at a density of 1×10^5 cells per well in 96-well plates. The culture was then incubated for 24 h at 37 °C, allowing for an additional 48 h incubation period. To assess the cytotoxic effects of the newly prepared ZnO-ZnS nanoparticles at concentrations of 2, 4, 6, 8, and 10 μg/mL, an in vitro cytotoxicity assay was conducted by using a

(3-(4,5-dimethylthiazol-2-yl)-2,5-diphenyl tetrazolium bromide) MTT assay. The cultured cells were exposed to the nanoparticles in a humidified chamber, containing 5% CO_2 at 37 °C. Following the incubation period, formazan crystals were produced by viable cells under the action of the MTT dye dissolved in 200 μL of DMSO. The absorbance was measured at 490 nm to quantify the cytotoxicity of the nanoparticles toward the HCT-116 cell line.

3. RESULTS AND DISCUSSION

3.1. FESEM, TEM, and EDS. The morphology and size of ZnO-ZnS nanoparticles were carefully examined by using FESEM and TEM, as shown in Figure 1. Figure 1a,b compares the morphology of ZnO and ZnS nanoparticles, confirming that both nanoparticles have a semispherical structure with some aggregation. However, the nanoparticles were finer with less aggregation in the case of ZnS (Figure 1b). The FESEM of the ZnO-ZnS heterostructure (Figure 1c) revealed that these nanoparticles exhibit a consistent and uniform shape with the size of 25−35 nm. The TEM image of ZnO-ZnS nanoparticles in Figure 1d confirmed that the nanoparticles are completely spherical, with the mean particle size around 25−30 nm. Importantly, Figure 1d demonstrates excellent monodispersity without any noticeable signs of agglomeration. Furthermore, particle size distribution of ZnO-ZnS nanoparticles was investigated, as depicted in Figure 2. The analysis revealed that approximately 86% of the particles fell within the size range of 12−29 nm. Moreover, the mean particle size was estimated to be around 25 nm, which aligns closely with the data obtained by using the Scherrer equation. The EDS spectrum of ZnO-ZnS (Figure 3) clearly revealed the presence of Zn, S, and O atoms, thereby providing conclusive evidence for the formation of ZnO-ZnS. Additionally, the absence of any peaks corresponding to impurity elements signified the remarkable purity of the synthesized nanomaterial.

3.2. FT-IR Spectroscopy. The FT-IR spectra of pure ZnO, ZnS, and ZnO-ZnS were analyzed to investigate the bonding
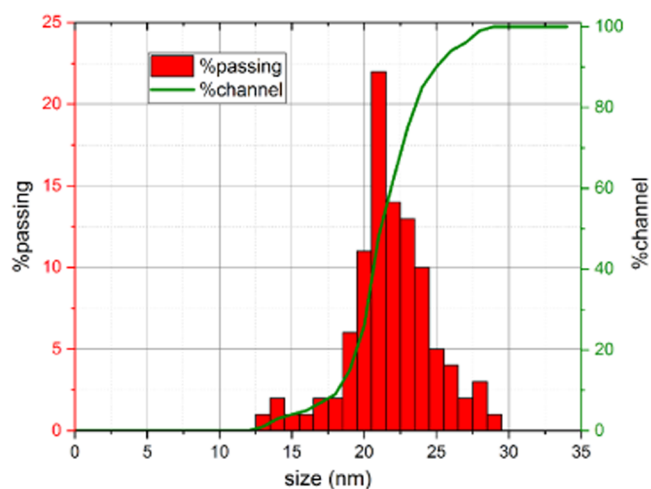
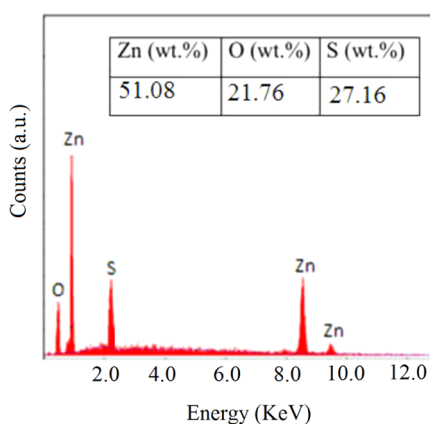**Figure 2.** Particle size distribution of the ZnO-ZnS heterostructure.

Figure 3. EDS analysis of ZnO-ZnS heterostructure.

nature in the prepared materials (Figure 4).[30−32] In the case of ZnO, notable peaks were observed at 427, 811, 1637, and 3433 cm^{-1} (Figure 4a). The absorption bands at 3421 and 1637 cm^{-1} in ZnS correspond to the stretching and bending vibrations, respectively, of O−H bonds in the adsorbed water
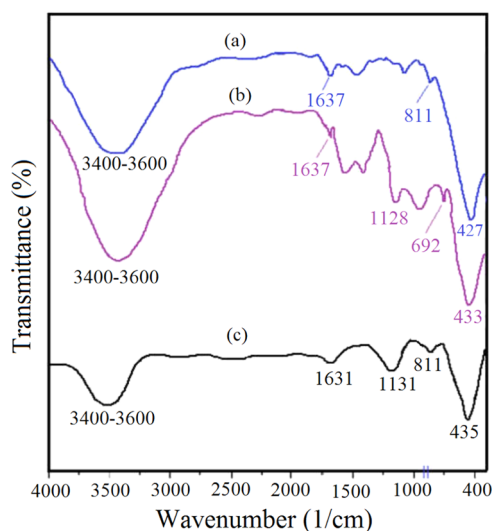

Figure 4. FT-IR spectra of (a) ZnO, (b) ZnS, and (c) the ZnO-ZnS heterostructure.

molecules (Figure 4b). Also, the peaks at 1128, 692, and 433 cm^{-1} confirmed the successful generation of ZnS nanoparticles. Finally, the presence of peaks at 435, 811, 1131, and 1631 and characteristic peaks in 3400−3600 cm^{-1} proved the coexistence of zinc sulfide and zinc oxide within the final prepared material (Figure 4c). It is worth noting that the broad peak observed at 3400−3600 cm^{-1} corresponded to the −OH group of adsorbed surface water on ZnO-ZnS.

3.3. XRD Analysis. The X-ray diffraction (XRD) analysis, as depicted in Figure 5, was conducted to assess the crystalline
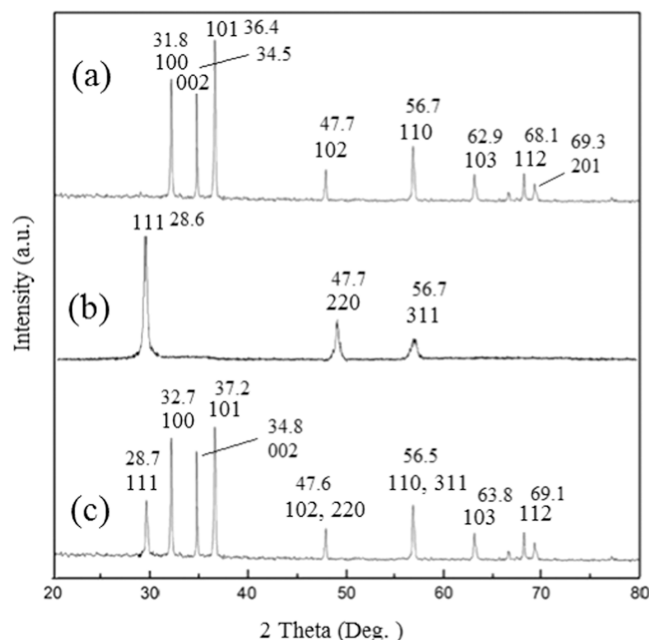

Figure 5. XRD patterns of (a) ZnO, (b) ZnS, and (c) ZnO-ZnS nanoparticles.

phase and purity of ZnO, ZnS, and ZnO-ZnS. The obtained results indicated that the samples possess a high degree of crystallinity, as evidenced by the presence of sharp peaks. In the XRD pattern of ZnO (Figure 5a), distinctive diffraction peaks were observed at the 2θ value of 31.8 34.5, 36.4, 47.7, 56.7, 62.9, 66.6, 68.1, and 69.3°. These peaks corresponded to the planes (100), (002), (101), (102), (110), (103), (200), (112), and (201), respectively. This investigation confirmed the formation of the hexagonal Wurtzite phase for ZnO. Additionally, the peaks for ZnS were detected at the 2θ value of 28.6 47.7, and 56.7, which corresponded to the reflection planes (111), (220), and (311), respectively (Figure 5b). Furthermore, the XRD pattern of ZnO-ZnS (Figure 5c) exhibited reflections at the 2θ values of 28.7, 32.7, 34.8, 37.2, 47.6, 56.5, 63.8, 66.3, 67.8, and 69.1, which corresponded to the reflections from crystal planes (111), (100), (002), (101), (102,220), (110,311), (103), and (112), respectively. Noticeably, the position of ZnO peaks was slightly shifted toward higher 2θ values compared to pure ZnO. The coexistence of ZnO and ZnS crystallites within the generated nanohybrid photocatalyst was distinctly discernible. In summary, the XRD analysis confirmed the excellent crystallinity and purity of the synthesized ZnO, ZnS, and ZnO-ZnS nanomaterials. The distinct diffraction peaks indicated the formation of the hexagonal Wurtzite phase of ZnO and the presence of hexagonal ZnS in the nanohybrid photocatalyst.[33,34] The

mean crystallite size of ZnO-ZnS nanoparticles was calculated by applying the Scherer equation (eq 1).

$$D = = k\lambda/\beta \cos\theta \tag{1}$$

where θ is the Bragg angle, β is the full width at half-maximum, λ is the X-ray wavelength (0.154 nm), k is the Scherrer constant (0.9), and D is the crystallite size. The mean crystal size of 28 nm was calculated for ZnO-ZnS.

3.4. DRS Analysis and Optical Properties.

DRS spectroscopy was employed as an effective method to evaluate the optical characteristics of ZnO-ZnS (Figure 6). Figure 6a
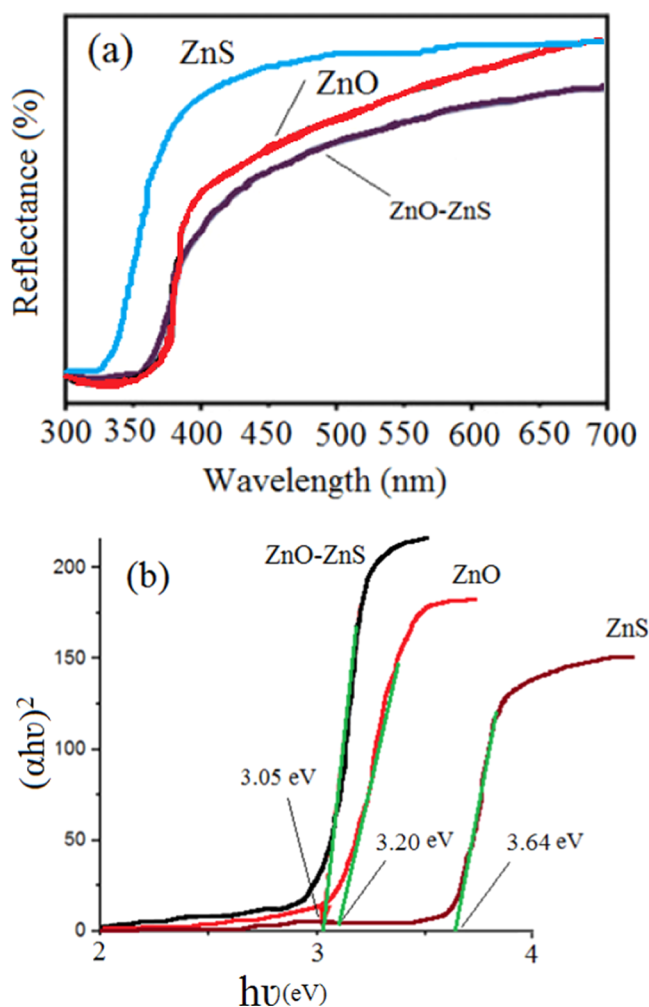

Figure 6. UV−visible reflectance spectra (DRS) of ZnO and ZnO-ZnS (a) as well as band gap analysis (b).

shows the UV−visible reflectance spectra of the ZnO, ZnS, and ZnO-ZnS nanomaterials. The absorption band of ZnO around 379 nm is due to the electron transition from the valence band of oxygen to the conduction band of zinc (O 2p to Zn 3d),[35] while a shift was observed in the absorption spectrum of ZnO-ZnS, which should be due to the characteristic absorption band of ZnS that locates at 220−350 nm.[36] The distinct absorption band in the UV−vis spectrum of the above nanoparticles could be used to calculate the corresponding band gap energy by using the Tauc model. By applying the Kubelka−Munk theory to diffuse reflection data, the absorption coefficients of the nanoparticles were obtained, and subsequently, the corre-

sponding optical band gap was attained by the linear portion of $(\alpha h\nu)^2$ vs $h\nu$ (Figure 6b). The plot is based on eq 2.

$$(\alpha h\nu)^2 = A(h\nu - E_g) \tag{2}$$

where A is a constant, E_g is the optical band gap, h is Planck's constant, and α is the absorption coefficient. The obtained band gap of the photocatalysts was determined as 3.20, 3.64, and 3.05 eV for pure ZnO, ZnS, and ZnO-ZnS, respectively.[37] It appears that the shift in the absorption band of ZnO-ZnS, when compared to that of ZnO, arises from the electronic interactions among ZnO and ZnS.

3.5. Catalytic Tests.

In order to find the optimal experimental conditions, a standard reaction was conducted to synthesize the chromene product by condensation of dimedone, benzaldehyde, and 4-hydroxycoumarin in the presence of ZnO-ZnS (0.01 g) in acetonitrile. To facilitate the reaction, the mixture was exposed to green light emitted by a diode with a maximum wavelength of 535 nm. The reaction took place at ambient temperature and at atmospheric pressure for a duration of 30 min (Table 1).

Table 1. Optimization Experiments for the Condensation Reaction

entry	light	ZnO-ZnS (g)	time (min)	yield (%)
1			30	7
2	green LED, 25 W		30	15
3	dark	0.01	30	38
4	20 × 1 W (white LED)	0.01	30	65
5	25 W (green LED)	0.01	30	87

Dimedone, benzaldehyde, and 4-hydroxycoumarin were condensed in acetonitrile under air at room temperature. 1 mmol of each reagent was used.

3.5.1. Effect of Catalyst, Solvent, Temperature, and Time.

Model reactions were run using different quantities of ZnO-ZnS to find the optimal catalyst amount. According to Figure 7, it was deduced that employing 0.01 g of photocatalyst yielded an impressive 87% yield. Interestingly, increasing amount of photocatalyst over this value had no positive impacts on yield and reaction time. Moreover, reducing the quantity of photocatalyst led to a lower yield, as depicted in Figure 7. The effect of solvent type on the progression of the reaction was also studied, as detailed in Table 2. To evaluate their effectiveness, we chose several commonly used solvents, namely, CH_3CN, $PhCH_3$, THF, and EtOH, and compared their results to the solvent-free case. The findings presented in Table 2 demonstrated that acetonitrile (CH_3CN) emerged as the most favorable solvent and provided the maximum yield of 87% within 30 min. Reaction temperature is also a significant parameter (Figure 8). Interestingly, the yield appears to be influenced by temperature and the optimum yield was achieved at ~25 °C after 30 min. As a result, room temperature was identified as the optimum temperature for all reactions. The study also focused on the impact of reaction time to get the optimum yield. As depicted in Figure 9, a duration of 30 min is sufficient to attain the maximum yield 87%. Interestingly, prolonging reaction time resulted in a little decrease in yield %, which may be attributed to catalyst poisoning.

3.5.2. Effect of the Irradiation Source and Presence of Oxygen.

The presence or absence of light and oxygen was also studied on the catalytic proficiency of ZnO-ZnS (Table 3). This experiment demonstrated that the reaction is strongly
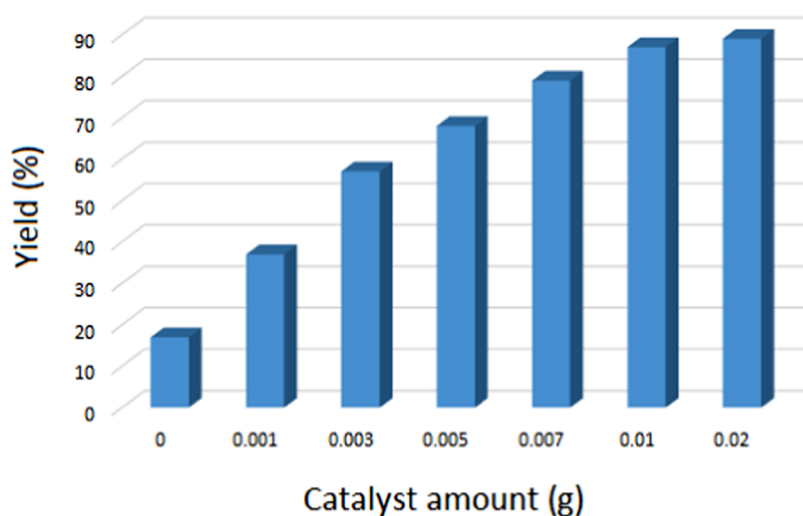
Figure 7. Effect of the photocatalyst amount on the condensation reaction.

Table 2. Optimization of Solvent Type on the Proficiency of the Desired Condensation Reaction

entry	ZnO-ZnS (g)	solvent	time (min)	yield (%)
1	0.01		180	83
2	0.01	water	180	42
3	0.01	toluene	180	68
4	0.01	ethanol	180	82
5	0.01	acetonitrile	30	87

Reaction conditions are described below Table 1. 5 mL of solvent was used in all cases.

Figure 8. Effect of reaction temperature.

Figure 9. Effect of the reaction time.

Table 3. Effect of Photocatalyst, Light, and Oxygen Gas on the Condensation Reaction

entry	green LED (25 W, λ 535 nm)	catalyst	air	time (min)	yield (%)
1	+		+	30	12
2	+	ZnO-ZnS	+	30	87
3	+	ZnO	+	30	58
4	+	ZnS	+	30	38
5	−	ZnO-ZnS	+	30	46
6	+	ZnO-ZnS	N_2	30	32

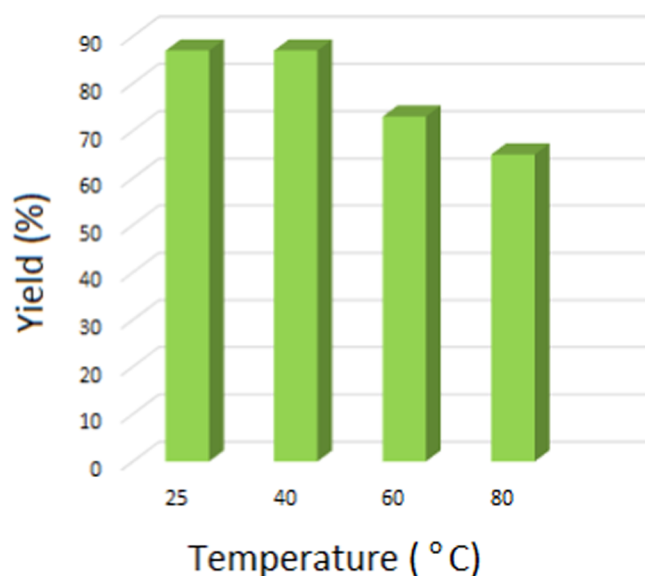Reaction condition is described below Table 1. 0.01 g of photocatalyst was used in 5 mL of acetonitrile.

dependent on the presence of photocatalyst, light, and oxygen gas. As depicted in Table 3, ZnO, ZnS, and ZnO-ZnS provided 58, 38, and 87% yields under the same experimental conditions (entries 2−4). This comparison revealed that the latter is the best among the examined mediators.

3.5.3. Role of Hole/Electron Scavengers. The impact of different scavengers on holes and electrons was assessed in the photocatalytic condensation reaction using ZnO-ZnS (Figure 10). Previous studies have suggested that hydroxyl radicals,
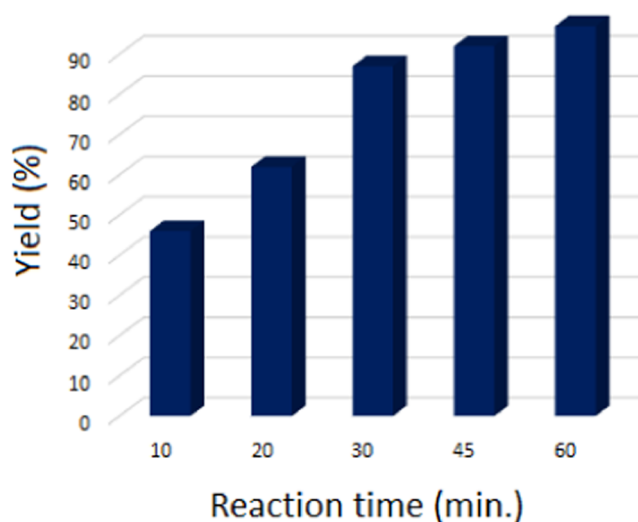
holes, and superoxide anion radicals play crucial roles in promoting the photocatalysis reaction.[38] In this experiment, isopropyl alcohol (IPA) effectively scavenged hydroxyl free radicals, resulting in a yield of 74%. Interestingly, the presence of p-benzoquinone (BQ), which scavenges $\cdot O_2^-$, yielded only yielded 37%. This finding clearly indicated the necessity of oxygen (O_2) during the photocatalytic process. Additionally, the presence of ethylenediaminetetraacetic acid (EDTA) led to a 12% decrease in yield due to the involvement of h$^+$ in the
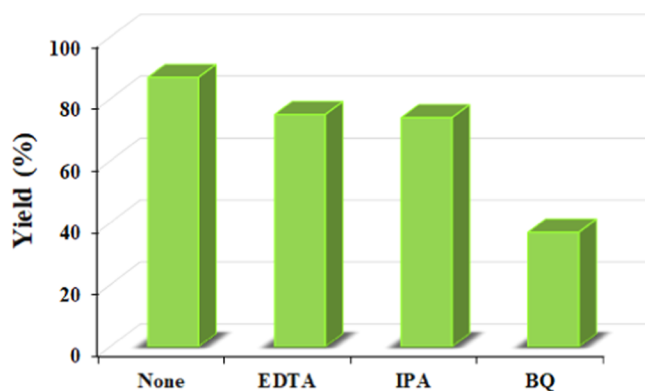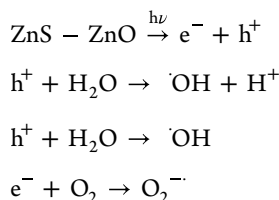
Figure 10. Effect of some common scavengers.

Figure 11. Schematic of the charge transfer process in the ZnO-ZnS heterostructure.

photocatalytic process. Hence, effective species such as OH$^\bullet$, $^\bullet$O$_2^-$, and h$^+$ are expected to be crucial in the current photocatalytic reaction. Based on these results, it can be concluded that the ZnO-ZnS photocatalyst facilitates progress of the reaction through the following reactions:

$$ZnS - ZnO \xrightarrow{h\nu} e^- + h^+$$

$$h^+ + H_2O \rightarrow \dot{}OH + H^+$$

$$h^+ + H_2O \rightarrow \dot{}OH$$

$$e^- + O_2 \rightarrow O_2^{-\dot{}}$$

Numerous investigations have consistently shown that the efficiency of photocatalysts relies heavily on the rate at which holes and electrons recombine, ultimately impacting the quantum yield of photocatalytic processes. Consequently, various strategies have been recommended to minimize the recombination rate.[39,40] The superior photoactivity observed in ZnO-ZnS compared to pure ZnO and ZnS can be attributed to its distinctive structural characteristics and enhanced generation of hole−electron pairs. In the nanohybrid ZnO-ZnS photocatalyst, the individual ZnO and ZnS components possess dissimilar energy levels for their conduction and valence bands. This permits the movement of holes and electrons between the two semiconductors. Furthermore, upon optical excitation, the photogenerated electrons gather in the lower-lying conduction band, while the holes accumulate in the valence band. As a result, the separation of charges augments the efficiency of the interfacial charge transfer process. A visual representation of these mechanisms is depicted in Figure 11.

3.5.4. Synthesis of Some Substituted Chromenes.
Versatility and generality of the present protocol was also encountered through the synthesis of some substituted chromenes. This is achieved by utilizing a range of substituted benzaldehydes possessing electron-donating/ withdrawing groups. Almost all benzaldehydes led to excellent performance and gave high yields in a short time (Table 4). These experiments proved that aldehydes containing electron-withdrawing substituents show superior reactivity than those with electron-donating substituents.

3.5.5. Proficiency of the Present Protocol over Other Methods.
Several studies have reported the synthesis of chromenes using various reaction conditions. In this study, we focused on comparing the presented condensation of benzaldehyde, dimedone, and 4-hydroxycoumarin as a representative example (Table 5). We compared the time,
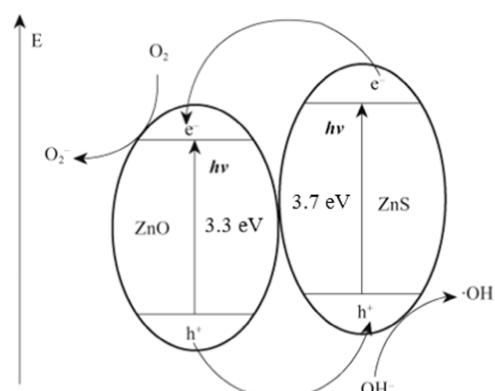
mol % of catalyst, and yield% to evaluate the effectiveness of our methodology. The results demonstrated several advantages, including use of a small amount of an environmentally friendly and cost-effective photocatalyst under mild reaction condition. This methodology provides a novel and efficient one-pot single-step synthesis of a broad range of chromenes under milder conditions, particularly under photochemical conditions with the illumination of an eco-friendly LED, which consumes minimal electrical energy.

3.5.6. Reusability of ZnO-ZnS.
To check reusability of ZnO-ZnS photocatalyst, it was separated after the first run, thoroughly washed with ethanol, dried and reused for the subsequent runs. The nanophotocatalyst underwent five consecutive cycles to estimate its reusability (Figure 12). Notably, the experiment disclosed a slight decline in the photocatalytic activity of ZnS-ZnO, resulting in an approximate decrease of 7% after five runs. This reduction can be attributed to surface poisoning of the photocatalyst. For further confirmation, the FT-IR spectra of ZnO-ZnS were compared before and after the fifth run, which revealed that the primary structure of ZnO-ZnS remained intact throughout the condensation reaction (Figure 13). Additionally, to ensure reproducibility of reaction, consecutive experiments were repeated and a negligible variation of ±3% was detected.

3.6. In Vitro Cytotoxicity and Cell Viability by MTT Assay.
The MTT assay was employed to investigate the cell viability of ZnS-ZnO. Notably, the results demonstrated a pronounced antiproliferative effect of this compound on HCT-116 human gastrointestinal cancer cells, as indicated by a significant difference ($P < 0.05$) (Figure 14a). In order to ascertain the concentration at which cell growth is inhibited, various concentrations of ZnO-ZnS ranging from 0 to 125 μg/mL were utilized. This analysis clearly exhibited a correlation between the inhibition of cell growth and concentration of the nanoparticles. Additionally, the toxicity of ZnO-ZnS nanoparticles toward the mouse fibroblast L929 normal cell line was also examined (Figure 14b). The findings revealed no noteworthy toxicity within the tested range of nanoparticle concentration, thereby highlighting their greater toxicity toward HCT-116 human gastrointestinal cancer cells compared to the normal cells.

4. CONCLUSIONS

A new efficient and environmentally friendly method is developed for the synthesis of chromeno[4,3-*b*]chromenes using visible light. The use of photoredox catalyst ZnO-ZnS

Table 4. Substrate Scope and Generality of the Condensation Reaction

$R_1 = NO_2$, F, Cl, Br, H, CH_3, OCH_3,
$R_2 = $ H, CH_3
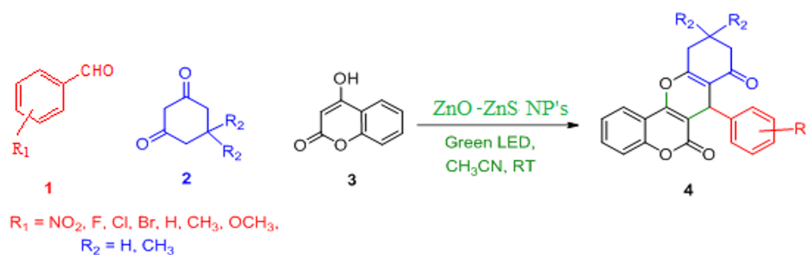
Aldehyde	Dimedone	Product	Yield (%)	M.P.
			87	221-223
			85	207-209
			77	227-230
			73	187-189
			77	241-243
			78	218-2198
			82	196-198

Reaction condition is described in experimental section. Reaction time is 30 min and 0.01 g of ZnO-ZnS used.

Table 5. Comparing the Catalytic Activity of ZnO-ZnS over Other Mediators in the Preparation of Chromeno[4, 3-b]chromene

catalyst	catalyst amount	time (h)	temp (°C)	solvent	yield (%)
Lewis acid-surfactant-combined catalyst[41]	10 mol %	1.5	70	H_2O (2.5 mL)	90
immobilized molybdic acid onto 3-chloropropyl-grafted magnetic silica-coated Fe_3O_4[42]	0.002 g	0.75	80		90
chlorosulfonic acid immobilized on $CuFe_2O_4$[43]	(0.05 g)	2.5	70	EtOH (5 mL)	90
ZrO_2[44]	10 mol %, 12.3 mg	0.5	80	H_2O (5 mL)	91
ZnO-ZnS [this work]	10 mg	30	r.t. green LED	- CH_3CN (5 mL)	87

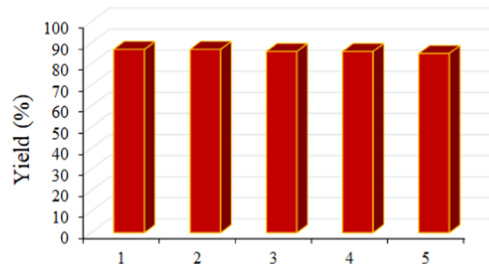Reaction conditions are described below Table 1.

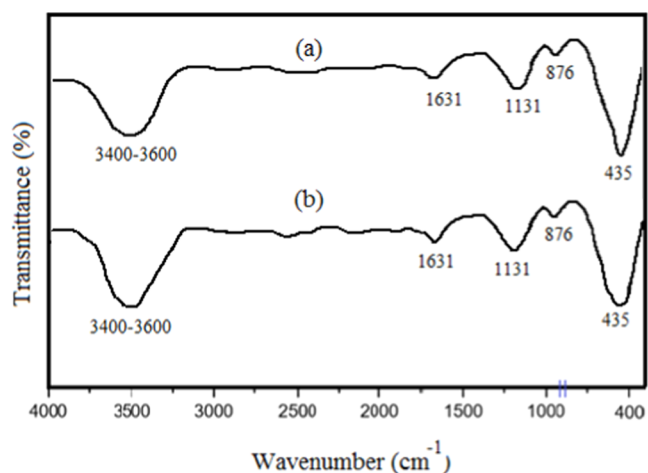**Figure 12.** Yield% as a function of reusability for ZnO-ZnS.

Figure 13. FT-IR spectra of fresh (a) and regenerated (b) ZnO-ZnS.
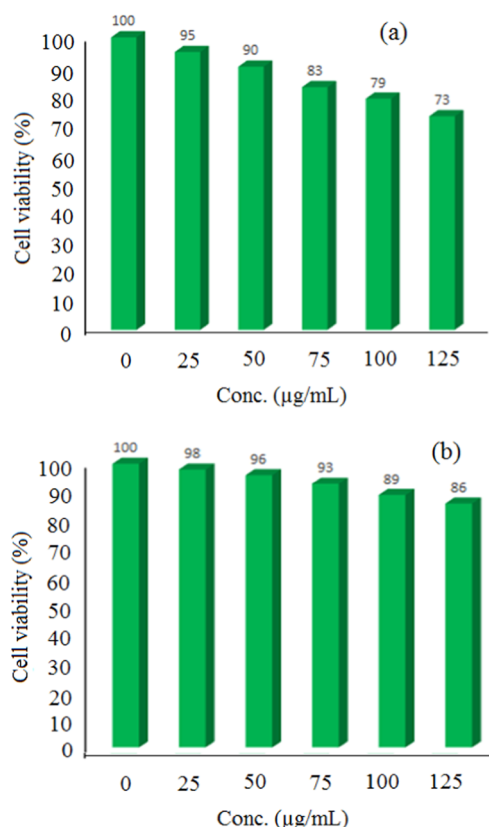

Figure 14. Cell viability of HCT-116 human gastrointestinal cancer cells (a) and normal cell line (L929) (b) in the presence of ZnO-ZnS over different concentrations ($n = 3$, $P < 0.005$).

offers a superior alternative that is both green and effective in promoting the target condensation reaction. We characterized the heterogeneous nanophotocatalyst through various techniques such as FESEM, TEM, UV−vis, DRS, EDS, XRD, and FT-IR. This new photocatalytic system possesses several key features that make it highly desirable. Mild conditions, easy workup, wide substrate tolerance, cost-effectiveness, and consistently high yields are noteworthy advantages. The ZnO-ZnS nanomaterial operates as a photocatalyst by initiating a series of electron transfer reactions under visible light via a radical mechanism, as demonstrated by employing various scavengers. Our investigation revealed that effective species $^\bullet O_2^-$ and $OH^\bullet$, along with h^+, play crucial roles in the photocatalytic synthesis of chromenes. However, further optical studies such as Mott−Schottky analysis, linear sweep voltammetry (LSV), and electrochemical impedance spectroscopy (EIS) are needed to unravel the mechanism of the p−n heterojunction formation. Importantly, the ZnO-ZnS photocatalyst can be reused up to five times without a significant loss of catalytic activity. Furthermore, we evaluated the cytotoxicity of ZnO-ZnS against the HCT-116 human gastrointestinal cancer cell line using the MTT assay across a range of concentrations. The results confirmed the potential of this nanomaterial as an effective agent against the targeted cell line and exhibited notable cytotoxicity. In summary, our developed ZnO-ZnS photocatalytic system offers a sustainable and efficient approach for synthesizing chromeno[4,3-*b*]-chromenes. Its unique properties, combined with its excellent performance and cytotoxicity against HCT-116 cells, position it as a promising candidate for further research and application in relevant fields.

■ ASSOCIATED CONTENT

Data Availability Statement
The data that support the findings of this study are openly available within the manuscript.

■ AUTHOR INFORMATION

Corresponding Author
Bing Liu − Department of Gastroenterological Surgery, Shandong Cancer Hospital and Institute, Shandong First Medical University and Shandong Academy of Medical Science, Jinan 250117 Shandong, China; ⊙ orcid.org/0009-0006-6780-4945; Email: bing.liu2002a@gmail.com, bingxuecaobaobao@163.com

Authors
Liqing Liu − Department of Gastroenterological Surgery, Shandong Cancer Hospital and Institute, Shandong First Medical University and Shandong Academy of Medical Science, Jinan 250117 Shandong, China

Longgang Wang − Department of Gastroenterological Surgery, Shandong Cancer Hospital and Institute, Shandong First Medical University and Shandong Academy of Medical Science, Jinan 250117 Shandong, China

Dong Sun − Department of Gastroenterological Surgery, Shandong Cancer Hospital and Institute, Shandong First Medical University and Shandong Academy of Medical Science, Jinan 250117 Shandong, China

Xu Sun − Department of Gastroenterological Surgery, Shandong Cancer Hospital and Institute, Shandong First Medical University and Shandong Academy of Medical Science, Jinan 250117 Shandong, China

Luguang Liu − *Department of Gastroenterological Surgery, Shandong Cancer Hospital and Institute, Shandong First Medical University and Shandong Academy of Medical Science, Jinan 250117 Shandong, China*

Weizhu Zhao − *Department of Oncology, Binzhou People's Hospital affiliated to Shandong First Medical University, Binzhou 256600 Shandong, China*

Reza Tayebee − *Department of Chemistry, School of Sciences, Hakim Sabzevari University, Sabzevar 96179- 76487, Iran*

Complete contact information is available at:
https://pubs.acs.org/10.1021/acsomega.3c06952

Author Contributions

L.L.: conceptualization. L.W.: project administration. D.S.: investigation, writing—original draft. X.S.: methodology, validation. L.L.: writing—review and editing. W.Z.: validation. R.T.: methodology, writing—review and editing.

Notes

The authors declare no competing financial interest.

■ REFERENCES

(1) Mandal, A. K.; Katuwal, S.; Tettey, F.; Gupta, A.; Bhattarai, S.; Jaisi, S.; Bhandari, D. P.; Shah, A. K.; Bhattarai, N.; Parajuli, N. Current research on zinc oxide nanoparticles: Synthesis, characterization, and biomedical applications. *Nanomaterials* **2022**, *12* (17), 3066.

(2) Lange, T.; Reichenberger, S.; Ristig, S.; Rohe, M.; Strunk, J.; Barcikowski, S.; Schlögl, R. Zinc sulfide for photocatalysis: White angel or black sheep? *Prog. Mater. Sci.* **2022**, *124*, No. 100865.

(3) Subhan, M. A.; Neogi, N.; Choudhury, K. P. Industrial manufacturing applications of zinc oxide nanomaterials: A comprehensive study. *Nanomanufacturing* **2022**, *2* (4), 265−291.

(4) Jalili, Z.; Koushki, E.; Ehsanian, A. H.; Tayebee, R.; Maleki, B. Synthesis, band gap structure and third order non-linear optical properties of zinc tungsten oxide nanocomposite using a single CW laser beam. *Front. Chem.* **2023**, *11*, No. 1152501.

(5) Guo, Z.; Huo, W.; Cao, T.; Liu, X.; Ren, S.; Yang, J.; Ding, H.; Chen, K.; Dong, F.; Zhang, Y. Heterojunction interface of zinc oxide and zinc sulfide promoting reactive molecules activation and carrier separation toward efficient photocatalysis. *J. Colloid Interface Sci.* **2021**, *588*, 826−837.

(6) Vlazan, P.; Ursu, D. H.; Irina-Moisescu, C.; Miron, I.; Sfirloaga, P.; Rusu, E. Structural and electrical properties of TiO2/ZnO core−shell nanoparticles synthesized by hydrothermal method. *Mater. Charact.* **2015**, *101*, 153−158.

(7) Preda, N.; Costas, A.; Enculescu, M.; Enculescu, I. Biomorphic 3D fibrous networks based on ZnO, CuO and ZnO−CuO composite nanostructures prepared from eggshell membranes. *Mater. Chem. Phys.* **2020**, *240*, No. 122205.

(8) Balachandran, S.; Prakash, N.; Thirumalai, K.; Muruganandham, M.; Sillanpää, M.; Swaminathan, M. Facile construction of heterostructured BiVO4 − ZnO and its dual application of greater solar photocatalytic activity and self-cleaning property. *J. Ind. Eng. Chem. Res.* **2014**, *53*, 8346−8356.

(9) Zhao, J.; Ge, S.; Pan, D.; Pan, Y.; Murugadoss, V.; Li, R.; Xie, W.; Lu, Y.; Wu, T.; Wujcik, E. K.; Shao, Q.; Mai, X.; Guo, Z. Microwave hydrothermal synthesis of in 2 O 3 -ZnO nanocomposites

and their enhanced photoelectrochemical properties. *J. Electrochem. Soc.* **2019**, *166*, H3074−H3083.

(10) Barrocas, B. T.; Ambrožová, N.; Kočí, K. Photocatalytic reduction of carbon dioxide on TiO2 heterojunction photocatalysts— a review. *Materials* **2022**, *15* (3), 967.

(11) Bahadoran, A.; Liu, Q.; Ramakrishna, S.; Sadeghi, B.; De Castro, M. M.; Cavaliere, P. D. Hydrogen production as a clean energy carrier through heterojunction semiconductors for environmental remediation. *Energies* **2022**, *15* (9), 3222.

(12) Feng, Y.; Li, J.; Ye, S.; Gao, S.; Cao, R. Growing COFs in situ on CdS nanorods as core−shell heterojunctions to improve the charge separation efficiency. *Sustainable Energy Fuels* **2022**, *6* (22), 5089−5099.

(13) Li, S.; Xu, W.; Meng, L.; Tian, W.; Li, L. Recent progress on semiconductor heterojunction-based photoanodes for photoelectrochemical water splitting. *Small Science* **2022**, *2* (5), No. 2100112.

(14) Zhihong, Y.; Ye, Y.; Pejhan, A.; Nasr, A. H.; Nourbakhsh, N.; Tayebee, R. A theoretical study on the pure and doped ZnO nanoclusters as effective nanobiosensors for 5-fluorouracil anticancer drug adsorption. *Appl. Organomet. Chem.* **2020**, *34* (4), No. e5534.

(15) Li, B.; Tayebee, R.; Esmaeili, E.; Namaghi, M. S.; Maleki, B. Selective photocatalytic oxidation of aromatic alcohols to aldehydes with air by magnetic WO3ZnO/Fe3O4. In situ photochemical synthesis of 2-substituted benzimidazoles. *RSC Adv.* **2020**, *10* (67), 40725−40738.

(16) Parvizi, E.; Tayebee, R.; Koushki, E. Mg-doped ZnO and Zn-doped MgO semiconductor nanoparticles; synthesis and catalytic, optical and electro-optical characterization. *Semiconductors* **2019**, *53*, 1769−1783.

(17) Jalili, Z.; Tayebee, R.; Zonoz, F. M. Eco-friendly synthesis of chromeno [4, 3-b] chromenes with a new photosensitized WO3/ZnO@NH2-EY nanocatalyst. *RSC Adv.* **2021**, *11* (29), 18026−18039.

(18) Raj, V.; Lee, J. 2H/4H-Chromenes—A versatile biologically attractive Scaffold. *Front. Chem.* **2020**, *8*, No. 623.

(19) Wen, Z.; Yang, K. C.; Deng, J. F.; Chen, L. Advancements in the Preparation of 4H-Chromenes: An Overview. *Adv. Synth. Catal.* **2023**, *365* (9), 1290−1331.

(20) Zheng, S. L.; Chen, L. Synthesis of 2 H-chromenes: recent advances and perspectives. *Org. Biomol. Chem.* **2021**, *19* (48), 10530−10548.

(21) Katiyar, M. K.; Dhakad, G. K.; Arora, S.; Bhagat, S.; Arora, T.; Kumar, R. Synthetic strategies and pharmacological activities of chromene and its derivatives: An overview. *J. Mol. Struct.* **2022**, *1263*, No. 133012.

(22) Djurišić, A. B.; He, Y.; Ng, A. Visible-light photocatalysts: Prospects and challenges. *Apl Mater.* **2020**, *8* (3), No. 030903, DOI: 10.1063/1.5140497.

(23) Liu, C.; Abbaspour, S.; Rouki, M.; Tayebee, R.; Jarrahi, M.; Shahri, E. E. Synergic promotion of the photocatalytic efficacy of CuO nanoparticles by heteropolyacid-attached melem: robust photocatalytic efficacy and anticancer performance. *Appl. Organomet. Chem.* **2022**, *36* (11), No. e6878.

(24) Jarrahi, M.; Maleki, B.; Tayebee, R. Magnetic nanoparticle-supported eosin Y salt [SB-DABCO@eosin] as an efficient heterogeneous photocatalyst for the multi-component synthesis of chromeno [4, 3-b] chromene in the presence of visible light. *RSC Adv.* **2022**, *12* (45), 28886−28901.

(25) Almojil, S. F.; Ali, M. A.; Almohana, A. I.; Alali, A. F.; Almoalimi, K. T.; Althahban, S.; Sharma, K.; Ahmed, A. N. Constructing a ZnO/CuCo2O4 pn heterojunction photocatalyst for efficiently hexavalent chromium−phenol detoxification and nitrogen fixation. *J. Phys. Chem. Solids* **2023**, *172*, No. 111057.

(26) Wannakan, K.; Khansamrit, K.; Senasu, T.; Nanan, S. Ultrasound-Assisted Synthesis of a ZnO/BiVO4 S-Scheme Heterojunction Photocatalyst for Degradation of the Reactive Red 141 Dye and Oxytetracycline Antibiotic. *ACS Omega* **2023**, *8* (5), 4835−4852.

(27) Das, A.; Patra, M.; Kumar P, M.; Bhagavathiachari, M.; Nair, R. G. Role of type II heterojunction in ZnO−In2O3 nanodiscs for enhanced visible-light photocatalysis through the synergy of effective

charge carrier separation and charge transport. *Mater. Chem. Phys.* **2021**, *263*, No. 124431.

(28) Das, A.; Kumar P, M.; Bhagavathiachari, M.; Nair, R. G. Hierarchical ZnO-TiO2 nanoheterojunction: A strategy driven approach to boost the photocatalytic performance through the synergy of improved surface area and interfacial charge transport. *Appl. Surf. Sci.* **2020**, *534*, No. 147321.

(29) Das, A.; Patra, M.; Kumar P, M.; Bhagavathiachari, M.; Nair, R. G. Defect-induced visible-light-driven photocatalytic and photo-electrochemical performance of ZnO−CeO2 nanoheterojunctions. *J. Alloys Compd.* **2021**, *858*, No. 157730.

(30) Chankhanittha, T.; Watcharakitti, J.; Piyavarakorn, V.; Johnson, B.; Bushby, R. J.; Chuaicham, C.; Sasaki, K.; Nijpanich, S.; Nakajima, H.; Chanlek, N.; Nanan, S. ZnO/ZnS photocatalyst from thermal treatment of ZnS: Influence of calcination temperature on development of heterojunction structure and photocatalytic performance. *J. Phys. Chem. Solids* **2023**, *179*, No. 111393.

(31) Yang, X.; Liu, H.; Li, T.; Huang, B.; Hu, W.; Jiang, Z.; Chen, J.; Niu, Q. Preparation of flower-like ZnO@ZnS core-shell structure enhances photocatalytic hydrogen production. *Int. J. Hydrogen Energy* **2020**, *45* (51), 26967−26978.

(32) Laokul, P.; Kanjana, N.; Ratchatanee, R.; Ruangjan, S.; Kotsarn, N.; Chingsungnoen, A.; Poolcharuansin, P. Preparation of AgBr decorated ZnO/ZnS nanocomposite for photocatalytic and anti-bacterial applications. *Mater. Chem. Phys.* **2023**, *295*, No. 127112.

(33) Tsai, Y. S.; Lin, X.; Wu, Y. S.; Chen, H.; Han, J. Dual UV light and CO gas sensing properties of ZnO/ZnS hybrid nanocomposite. *IEEE Sens. J.* **2021**, *21* (9), 11040−11045.

(34) Sundararajan, M.; Sakthivel, P.; Fernandez, A. C. Structural, optical and electrical properties of ZnO-ZnS nanocomposites prepared by simple hydrothermal method. *J. Alloys Compd.* **2018**, *768*, 553−562.

(35) Li, L.; Yang, H.; Yang, P. Lutetium-Doped ZnO to Improve Photovoltaic Performance: A First-Principles Study. *ACS Appl. Electron. Mater.* **2022**, *4* (12), 6253−6260.

(36) Study of far infrared optical properties and, photocatalytic activity of ZnO/ZnS heteronanocomposite structure.

(37) Dolgonos, A.; Mason, T. O.; Poeppelmeier, K. R. Direct optical band gap measurement in polycrystalline semiconductors: A critical look at the Tauc method. *J. Solid State Chem.* **2016**, *240*, 43−48.

(38) Jarrahi, M.; Tayebee, R.; Maleki, B.; Salimi, A. One-pot multicomponent green LED photoinduced synthesis of chromeno [4, 3-b] chromenes catalyzed by a new nano-photocatalyst histaminium tetrachlorozincate. *RSC Adv.* **2021**, *11* (32), 19723−19736.

(39) Koe, W. S.; Lee, J. W.; Chong, W. C.; Pang, Y. L.; Sim, L. C. An overview of photocatalytic degradation: photocatalysts, mechanisms, and development of photocatalytic membrane. *Environ. Sci. Pollut. Res.* **2020**, *27*, 2522−2565.

(40) Gao, W.; Lu, J.; Zhang, S.; Zhang, X.; Wang, Z.; Qin, W.; Wang, J.; Zhou, W.; Liu, H.; Sang, Y. Suppressing photoinduced charge recombination via the Lorentz force in a photocatalytic system. *Adv. Sci.* **2019**, *6* (18), No. 1901244.

(41) Pradhan, K.; Paul, S.; Das, A. R. Fe (DS) 3, an efficient Lewis acid-surfactant-combined catalyst (LASC) for the one pot synthesis of chromeno [4, 3-b] chromene derivatives by assembling the basic building blocks. *Tetrahedron Lett.* **2013**, *54* (24), 3105−3110.

(42) Khosravian, F.; Karami, B.; Farahi, M. Synthesis and characterization of molybdic acid immobilized on modified magnetic nanoparticles as a new and recyclable catalyst for the synthesis of chromeno [4, 3-b] chromenes. *New J. Chem.* **2017**, *41* (20), 11584−11590.

(43) Vajar, S.; Mokhtary, M. Nano-CuFe$_2$O$_4$@SO$_3$H catalyzed efficient one-pot cyclo-dehydration of dimedone and synthesis of chromeno [4, 3-b] chromenes. *Polycyclic Aromat. Compd.* **2019**, *39* (2), 111−123.

(44) Zonouzi, A.; Rahmani, A.; Miralinaghi, P. S. Nano-Sized Zirconium Dioxide Promoted Synthesis of Some Fused Polycyclic-2H-Chromenes. *Org. Prep. Proced. Int.* **2017**, *49* (5), 434−442.